Microalloying ’25: International Symposium on Microalloying
2–5 June 2025
Vail, Colo., USA
10.33313/302/003

Effect of Nickel Alloying on Strength and Toughness Properties in Heavy Plate Steels

Charles Stallybrass[1], Jörg Wiebe[1], Juliane Mentz[1], Andreas Kern[2] and Hardy Mohrbacher[3]

[1]Salzgitter-Mannesmann
[1]Forschung GmbH,
Ehinger Strasse 200, 47259 Duisburg, Germany

[2]Thyssenkrupp Steel Europe AG
Kaiser-Wilhelm-Str. 100, 47166 Duisburg, Germany

[3]NiobelCon BV
Swaenebeecklaan 5, 2979 Schilde, Belgium
Email: hm@niobelcon.net

INTRODUCTION

Heavy plates used for offshore applications are often confronted with harsh environments, demanding superior toughness properties, especially in mid plate thickness and weld HAZ. Typically, such HSLA steels are niobium microalloyed and produced to a minimum yield strength ranging from 350 to 460 MPa by TMCP or rolling normalizing heat treatment processes. Experience shows that the required properties can often only be achieved by nickel alloying of up to 1.0 percent [1].

The significant extension of the austenite phase field by nickel alloying in combination with its low diffusivity in the austenite lattice delays the austenite-to-ferrite transformation towards lower temperature or extended times [2]. The resulting undercooling causes an increased ferrite nucleation rate and decreased ferrite growth rate, leading to a general refinement of the ferrite microstructure. It has been postulated [3] that the refining effect of nickel alone and at slow cooling rates is rather modest. Accelerated cooling from temperatures above A_{r3} induces a similar undercooling effect and refinement mechanisms. However, this is not always an option for very heavy plate gages especially in the mid-thickness region. While nickel’s alloy effect in combination with that of accelerated cooling can act in synergy, the excessive application of both parameters might cause, however, the formation of undesirable coarse bainite structures during the transformation from equiaxed austenite. One of the most prominent effects of nickel alloying in carbon steels is its improvement of toughness independent of grain size. Therefore, nickel alloying is often considered in plates of very heavy gage, where strong TMCP rolling is not possible for practical reasons and especially when toughness requirements apply to the mid-thickness region. Furthermore, beneficial effects of nickel have been reported in the heat affected zone (HAZ) caused by welding, which often exhibits low toughness performance especially in the coarse-grained sub-zone (CGHAZ).

This study investigates typical HSLA plate steel compositions with a nominal strength of 355 MPa used for structural applications in the offshore and wind energy sector. Starting from a peritectic microalloyed HSLA steel with ferritic-pearlitic microstructure, the carbon content is systematically reduced while the alloy content of nickel and copper is increased, thereby shifting weldability from zone II (“weldable”) into zone I (“easy to weld”) according to the Graville diagram [4] (Figure 1a). Two different plate gages (30 and 80 mm) have been rolled. Thus, implicitly also the effect of austenite conditioning is investigated. The results indicate that superior performance can be achieved by increasing the nickel content, especially for the heavier plate gages. These improvements apply to the as-rolled steel as well as to the HAZ properties. A detailed analysis aims to explain the observed effects based on microstructural analysis and builds a framework for allowing optimized alloy design.

Keywords: Strengthening mechanisms, transformation behavior, carbon-rich particles, heat affected zone properties, toughness, CTOD, Lüders deformation, continuous yielding

EXPERIMENTAL

The investigation of the nickel influence on relevant properties was done for steels containing up to 1.0 wt.% Ni. Therefore, laboratory heats of each 300 kg weight were produced by vacuum induction melting with four different alloy compositions according to the chemical compositions shown in Table 1. Besides nickel, also carbon (0.14−0.07%), copper (0−0.5%), and manganese (1.35−1.50%) additions were varied. Thereby, the reduction of carbon is mitigated by increasing additions of Ni, Cu and Mn to maintain sufficient strength. The carbon equivalent in all investigated steels is mostly kept within the limit defined by EN10225. The microalloy concept employing Nb and Ti was kept constant. The role of niobium is mainly to control the grain size during TMCP or normalizing processes. The aim of the near-stoichiometric nitrogen to titanium addition is to establish a fraction of TiN particles that prevent excessive grain coarsening in the heat affected zone (HAZ) during welding. The general alloying strategy of these laboratory heats, besides investigating the mere influence of nickel, is demonstrated by the Graville diagram in Figure 1a. The steel alloys consistently progress towards better weldability from alloy 1 to 4. The alloy concepts do not strictly align with the requirements of the specification DIN EN10225 as the Cu and Ni contents in alloys 3 and 4 where chosen on the high side. The Norsok standard, however, does allow a nickel content of 1 wt.%. It should be mentioned that the addition of 0.11 wt.% Cr to these laboratory steels was needed because of the use of nitrided ferro chrome to adjust the nitrogen level to 50 ppm that otherwise would be too low when using laboratory vacuum melting. A chromium addition of 0.11 wt.% contributes 2 points to the CEV, which would be saved in industrial heats.

Cast ingots of 235 mm thickness were rolled on a reversing single-stand 1000 t two-high laboratory rolling mill to plate gages of 30 and 80 mm, respectively. Rolling was performed in two stages according to appropriate TMCP schedules. Pre-rolling occurred in the temperature range of 1090 to 960 °C while finish rolling was done between 880 and 790 °C, followed by air cooling. Experience showed that the practiced laboratory rolling schedules replicate industrial plate rolling with good accuracy. For investigating the properties in the heat affected zone (HAZ), plates were welded by submerged arc welding according to the parameters shown in Figure 1b. The tested steels were welded against dummy plates of the same gage. The welds in the 30- and 80-mm thick plates were composed of 21 and 33 weld passes, respectively, and supported by a backing strip for root welding. The plate edges were square beveled, facilitating Charpy V-notch and CTOD testing along the fusion line (FL) and at a distance of 2 mm (FL+2). These positions represent the coarse-grained heat affected zone (CGHAZ) and the subcritical heat affected zone (SCHAZ).

Base material and weld seams were metallographically characterized using light optical microscopy after HNO_3 etching to determine phase composition and grain sizes. The CGHAZ was additionally investigated using scanning electron microscopy by taking 280 pictures at 3000x magnification on each cross section for determining the volume fraction of carbon-rich phases by automated image analysis. Tensile testing was used to determine the mechanical properties of the as-rolled steel in transverse direction. Charpy V-notch testing was performed at -20, -40, and -60 °C at mid- as well as quarter thickness positions. For the weld seams, Charpy testing was performed at -50 °C with notches at cap, middle, and root positions. Furthermore, crack tip opening displacement (CTOD) tests were done in the at -20°C using single-edge notched bar (SENB) specimens. Through thickness notches were placed in the CGHAZ of the specimens.

Table 1: Chemical composition of experimental steels in wt.% and carbon equivalent (CEV).

Alloy	C	Si	Mn	P	S	Al	Cu	Cr	Ni	Nb	Ti	N	CEV
1	0.14	0.2	1.34	<0.015	<0.0015	0.03	0	0.11	0	0.03	0.015	0.005	0.38
2	0.12		1.45				0.20		0.30				0.41
3	0.09		1.47				0.51		0.49				0.42
4	0.07		1.51				0.52		0.98				0.44

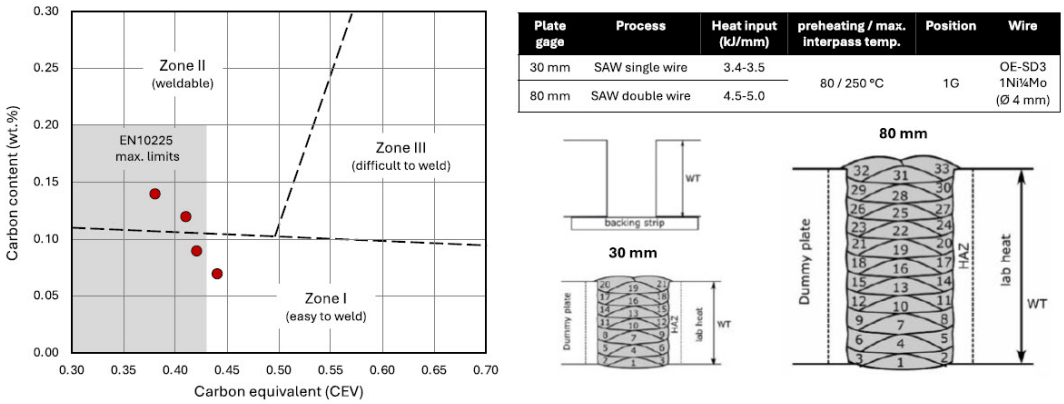

Figure 1: (a) Position of the investigated alloy concepts in the Graville diagram and maximum carbon / CEV limits defined in standard EN10225. (b) Submerged arc welding (SAW) procedure applied to the experimental plate steels.

RESULTS

Properties of as-Rolled Plate Steel

Figure 2 shows representative light optical micrographs of the four alloy concepts after rolling to 30- and 80-mm plate thickness. The phase composition of alloy 1 mainly comprises polygonal ferrite and pearlite in a ratio of approximately 75:25%. With decreasing carbon and simultaneously increasing the alloy content of Ni, Cu and Mn, an increasing fraction of bainite (and martensite in plates of 30 mm gage) is formed at the expense of pearlite, while the polygonal ferrite fraction remains between 70 and 80%. The average grain size decreases from ASTM 7.5 in alloy 1 towards ASTM 9 in alloy 4. These features indicate that the transformation from austenite to ferrite must be delayed with increasing alloy content of Ni, Cu, and Mn.

The tensile strength increases from alloy 1 to 4 (Figure 3) and is generally 30–40 MPa higher in the 30 mm plates. The yield strength does not show such a clear correlation with the CEV, particularly in the 30 mm plates. All steels except alloy 4 rolled to 30 mm plate gage feature pronounced yielding followed by Lüders deformation varying between 0.5 and 4 percent (see inserts in Figure 3). Alloy 4 in gage 30 mm shows continuous yielding with strong initial work hardening gaining approximately 80 MPa from the onset of yielding to Rt0.5. All steels except alloy 1 in 80 mm plate gage fulfil the minimum specified requirements of yield and tensile strength according to EN10225. The minimum required total elongation of 22% is reached for all steels. It is apparent that the yield strength and Lüders elongation are significantly larger for alloys 2–4 in the 80 mm plates, as compared to the 30 mm plates. Particularly the 80 mm plate of alloy 3 has a very favorable combination of strength and total elongation.

The Charpy toughness measured at quarter- and mid-thickness positions behaves clearly different for the two plate gages (Figure 4). The absorbed impact energy is generally higher in the 80 mm plates reaching the best performance with alloy 3. Thus, both elongation and toughness indicate a very good ductility for that steel. In the 30 mm plates, alloys 3 and 4 show the lowest toughness performance. Apparently, the higher addition of Cu and Ni in these two alloys, in combination with the relatively faster cooling when rolling to 30 mm plate gage, produces microstructural constituents that are unfavorable to toughness. Alloy 2 exhibits the best toughness at -60 °C in mid-thickness position. The observations suggest that nickel alloying must be matched to the plate gage and the prevailing cooling conditions after rolling. In that way, superior combinations of strength and toughness can be achieved.

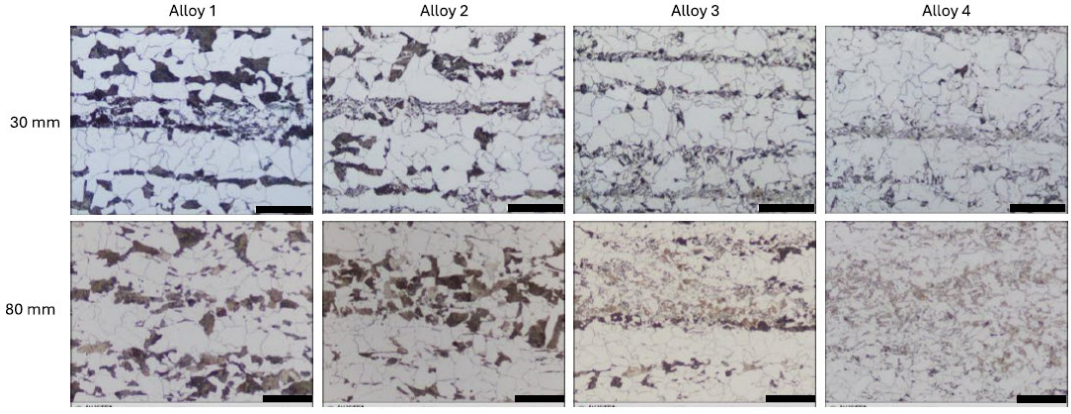

Figure 2: Light optical micrographs of experimental steels in as-rolled condition at quarter thickness position (HNO_3 etching, scale marker = 50 µm).

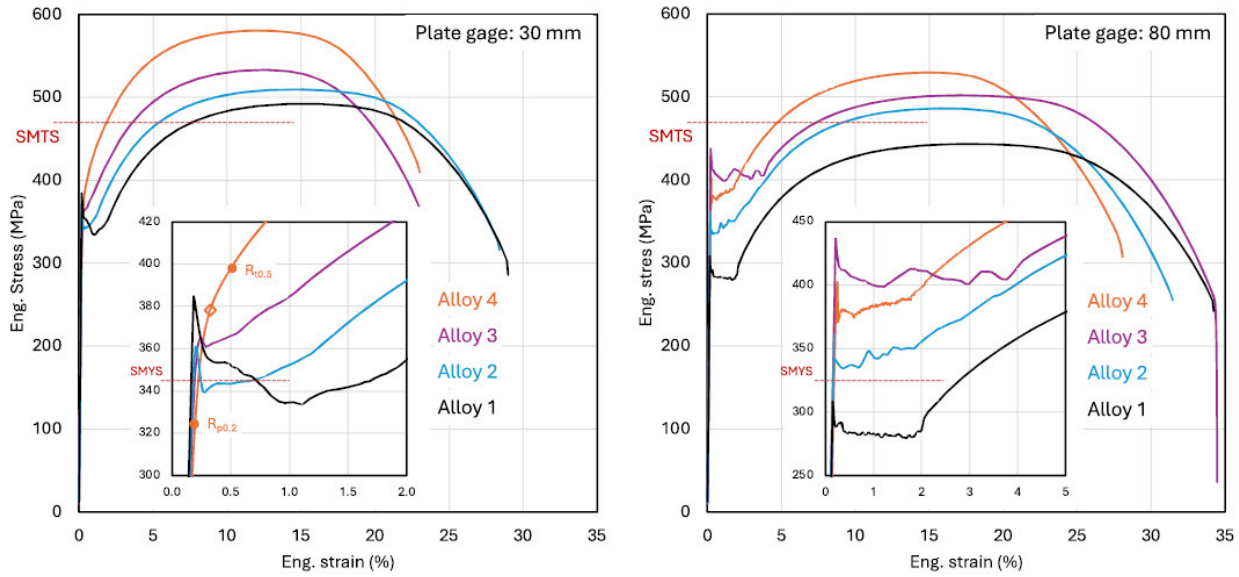

Figure 3: Engineering stress-strain curves of all investigated steels with close-up on the early yielding behavior (SMYS, SMTS represent minimum specified yield and tensile strength levels for S355 according to EN 10225).

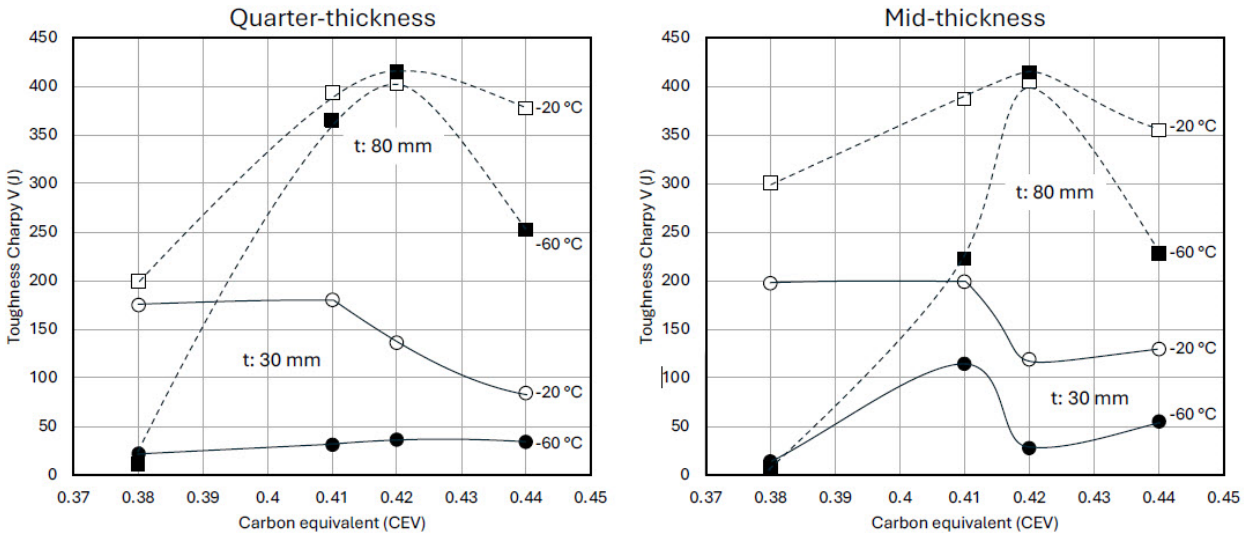

Figure 4: Charpy toughness performance in the temperature range of -20 to -60 °C for the as-rolled steels in quarter- and mid-thickness position.

Properties in the Heat Affected Zone

A representative macrograph of weld seams produced with 80 mm plate gage is shown in Figure 5a. Hardness (HV10) scans were taken across all weld sections. CGHAZ toughness was evaluated using Charpy samples with notches positioned at the fusion line. Light optical microscopy of the CGHAZ revealed that alloy 1 featured the largest (ASTM 3, Figure 5b) while alloys 3 and 4 had the finest (between ASTM 4 and 6, Figure 5c) prior austenite grain sizes. Scanning electron micrographs of the CGHAZ are shown in Figure 6 for all four alloys and both plate gages. Such images were quantitatively evaluated, assisted by image processing software to reveal the volume fractions and sizes of carbon-rich phases such as pearlite and martensite. The CGHAZ in the 30 mm plate of alloy 1 contains a high pearlite share (~13%) and a small fraction of MA phase (<2%). In the CGHAZ of alloys 2–4 the total amount of carbon rich phase is lower (5-11%) than in alloy 1 and the ratio of pearlite and MA is nearly equal. The CGHAZ of alloy 3 comprises the largest amount of MA phase (~7%) and the particles also have the biggest size. However, the CGHAZ of the 80 mm plates contains only between 4 and 6 percent carbon-rich phases for all alloys. The share of MA phase is thereby generally less than 0.5%. The mean volume fraction of MA phase particles in the CGHAZ of the 80 mm plates is less than half of that found in the CGHAZ of the 30 mm plates. However, that criterion does not consider the morphology of MA phase. In some of the micrographs the MA phase appears mostly with needle-shaped morphology (Figure 6: alloy 1, alloy 3 gage 30 mm), while in others the particles have a more compact shape.

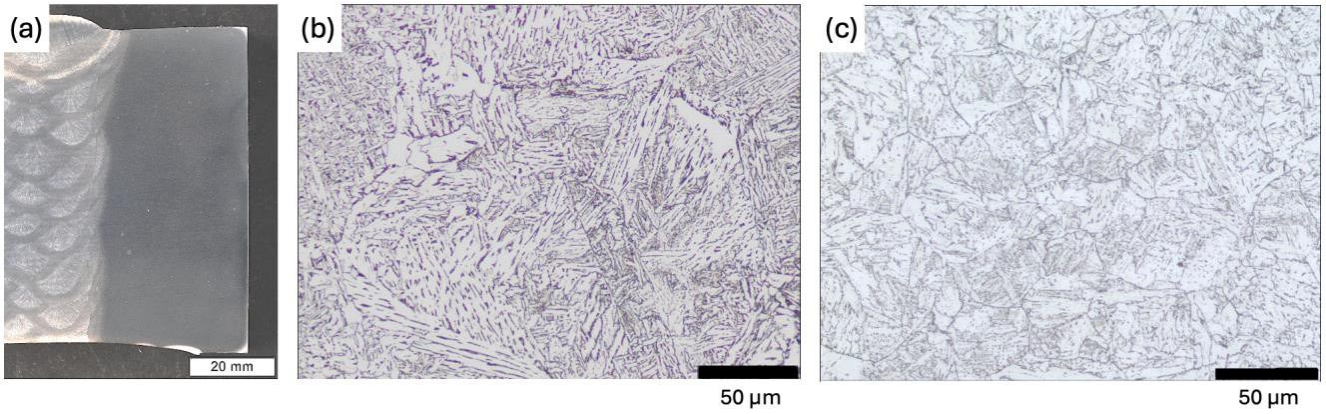

Figure 5: (a) Weld layer build up in the 80 mm plate gage; light optical micrographs after etching with HNO_3 of the CGHAZ in alloy 1 (b) and alloy 4 (c) revealing the prior austenite grain structure.

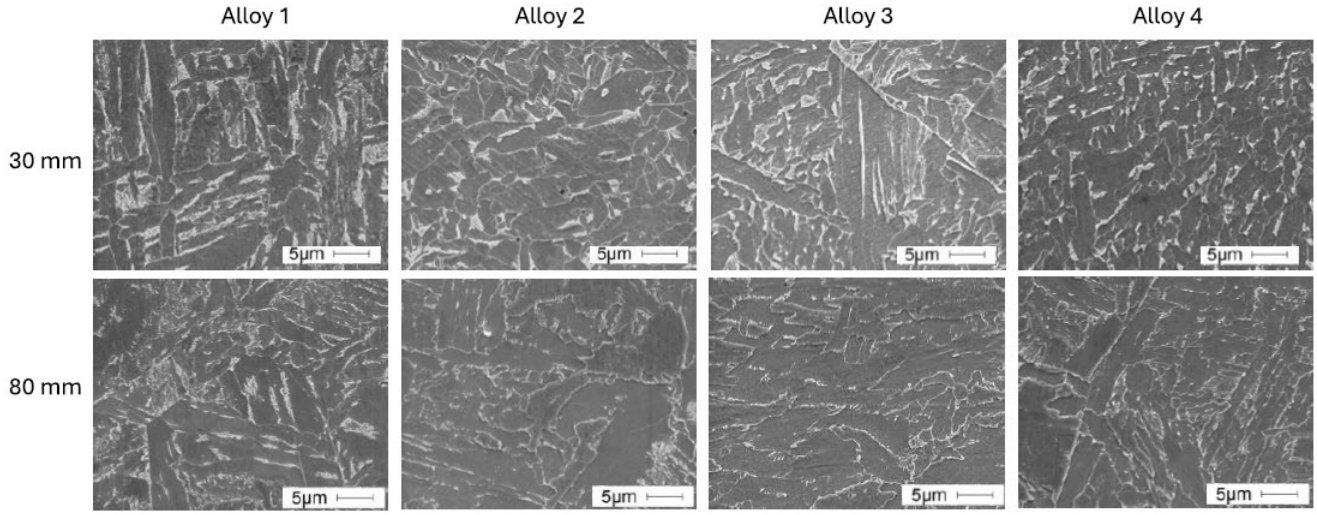

Figure 6: Scanning electron micrographs of the CGHAZ identifying the morphology and distribution of carbon-rich phases (bright contrast).

The evolution of hardness as a function of the CEV is similar in the base metal and the HAZ for both plate gages (Figure 7a). The hardness in the HAZ is 40-60 HV higher than that of the base metal. The alloys become better hardenable with increasing CEV, and this effect is more prominent for the 80 mm plate gage welded with a larger heat input.

Charpy toughness was measured in the weld cap, center and root area at a testing temperature of -50 °C. The average values for notches in the CGHAZ and FL+2 position are shown in Figure 7b. These average values are much better than the minimum of 36 J required by EN10225. The toughness evolution as a function of the CEV is principally similar with exception of the CGHAZ toughness in the 30 mm plate of alloy 4. It is worth noting that the HAZ toughness in the 30 mm plates is higher than the base metal toughness. CTOD measured in the CGHAZ and FL+2 position of the 30 mm plates shows qualitatively similar behavior. Only alloy 1 comprises a large discrepancy in CTOD value between the CGHAZ and the FL+2 position. The CTOD values measured in the CGHAZ at -30 °C are lower than those at -20 °C. Under all tested conditions, alloy 2 presents the best performance while for alloy 3 a decline is observed. This behavior is congruent with the one found for toughness. In the 80 mm plates CTOD was only measured in the CGHAZ at -20°C. The values for alloys 1 and 2 are below 0.2 mm and increase to above 0.4 mm for the steels with higher nickel content.

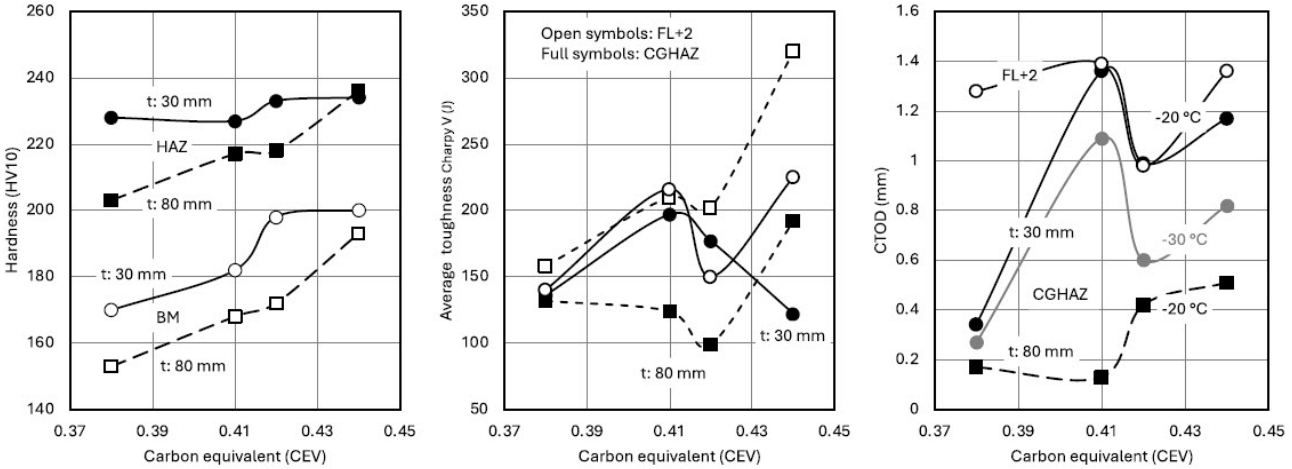

Figure 7: (a) Average hardness values (HV10) comparing HAZ with the base metal (BM); (b) Average Charpy toughness values at -50 °C for samples notched at the FL and FL+2 position; (c) Crack tip opening displacement (CTOD) measurements performed at -20 and partially -30 °C in the CGHAZ and partially FL+2 position.

DISCUSSION

The results generally confirm that the intended optimization of alloy concepts for S355 heavy plate steel in the relevant aspects of base metal properties and weldability can be realized. Reducing the carbon content and refining the grain size are standard practice for improving low-temperature toughness. Nickel alloying additionally improves low-temperature toughness. The strength loss related to reducing the carbon content in the investigated steels is counterbalanced mainly by the addition of nickel and copper as well as the slightly raised manganese content. These alloying elements in first place contribute to solid solution strengthening which according to Pickering [5] can be estimated as $\sigma_s = 33\times Ni\% + 40\times Cu\%$. With the chosen alloy additions, the expected solute contributions are 18, 36, and 53 MPa for alloys 2, 3, and 4, respectively. Grain refinement is promoted by microalloying in combination with austenite conditioning. The microalloying concept relying on niobium and titanium is identical in all alloys. It is expected that the major share of titanium forms nitride particles which are intended to control austenite grain size in the CGHAZ. Niobium acts either by solute drag or strain induced precipitates during austenite conditioning. Austenite conditioning and thus precipitation of niobium is more pronounced in the 30 mm plates. However, in both plate gages, part of the niobium remains in solid solution after rolling has been finished and thus has the propensity to precipitate during or after phase transformation. These nano-sized niobium precipitates can significantly contribute to strength. Solute niobium also delays the phase transformation by solute drag effects on the phase front. Austenite stabilizing elements such as nickel, copper and manganese reduce the transformation temperature. This increases the nucleation potential of ferrite and as such contributes to refinement. Strain accumulation during austenite conditioning acts as a driving force for transformation of proeutectoid ferrite. This early forming polygonal ferrite causes partitioning of austenite stabilizing elements as well as interstitials to remaining austenite islands. This might cause the formation of undesirable coarse bainite structures during the transformation from equiaxed austenite or small martensite / MA particles.

These effects can be clearly distinguished in the investigated steels. The stronger austenite conditioning applied to roll the 30 mm plate gage evidently results in the formation of LTT phases in the alloys containing nickel and copper. This reflects in the yielding behavior (Figure 3) changing from pronounced yielding (alloys 1-3) to continuous yielding (alloy 4). The magnitude of the Cottrell effect diminishes with increasing Ni and Cu content from around 50 MPa in alloy 1 to only 5 MPa in alloy 3 and finally completely disappears in alloy 4. Simultaneously, the Lüders strain diminishes from around 2 percent in alloy 1 to 0.6 percent in alloy 3. The interpretation of these observations suggests that the number density of instantly mobile dislocations increases from alloy 1 to alloy 4 corresponding to the amount of LTT phase dispersed in the ferrite matrix, ultimately allowing continuous yielding in alloy 4. However, the increasing presence of LTT phase is considered to be responsible for the lower toughness performance in the 30 mm plates of alloys 3 and 4. The yielding characteristics of the 80 mm plates suggests a much lower share of LTT phase. All steels show pronounced yielding and Lüders elongation is more substantial than in the thinner-gaged steels. The 80 mm plates of alloys 2–4, despite less strong austenite conditioning, feature higher yield strength than the 30 mm plates while alloy 1 did not fulfil the specified minimum strength criterion.

An approach for identifying the different contributions to yield strength was applied to the present HSLA steels using a method described in [6]. Thereby the theoretical yield point (YP) represents the sum of base strength, solid solution strengthening and Hall-Petch effect. Contributions of precipitation strengthening and the Cottrell effect add to the YP causing pronounced yielding. Accordingly, the difference between lower yield stress (LYS) and YP is considered as the contribution originating

from the nano-sized precipitate population. Figure 8a presents the result of this analysis for all produced plate steels. YP increases consistently with the CEV showing a similar pattern for both plate gages. The strength increments are caused by increasing solid solution strengthening due to Ni and Cu (as determined above) as well as grain refinement. Thus, the Hall-Petch contribution can be estimated as 35, 58, and 103 MPa for alloys 2–4 in the 30 mm plates. As expected, in the 80 mm plates, the grain refinement contribution is reduced to 23, 42, and 64 MPa, respectively. Comparing the YP for the two gages of the same alloy presents an advantage in the 30 mm plates of 56, 68, 72, and 95 MPa for alloys 1–4, respectively, indicating that beyond the degree of austenite conditioning, alloying by nickel and copper produces additional grain refinement due to transformation delay and related promotion of ferrite nucleation.

Precipitation strengthening is the similar at 180 MPa in both plate gages of alloy 1. This is a high value considering the relatively low niobium content suggesting that the particles must be very small in size to generate a large particle number density [7]. Using the Orowan approach [8], an average particle size of 5 nm would generate such a strength increase for an assumed amount of 200 ppm niobium being left for precipitation after finish rolling. Precipitation strengthening significantly declines in the 30 mm plates with increasing nickel and copper content to a value of only 30 MPa in alloy 4. The instantly mobile dislocations in alloy 4 strongly interact with precipitates upon yielding at $R_{p0.2}$ and subsequently produce work hardening by Orowan looping. This instant work hardening effect reaches its maximum at about 0.3 percent strain thereby increasing the flow stress by around 60 MPa (see Figure 3, diamond symbol). Decreasing precipitation strengthening is likely caused by less favorable conditions for the particle forming mechanism in the 30 mm plates with higher CEV. A reduced transformation temperature is the prospective reason for a slower precipitation kinetics which is controlled by temperature and time. On the contrary, the slower cooling rate in the 80 mm plates is favorable to precipitation kinetics. Precipitation strengthening reaches a maximum contribution of 221 MPa in alloy 3 indicating that an optimum in terms of precipitation completeness and particle size has been achieved. Precipitation appears to be incomplete only in alloy 4, which again is likely related to a lower transformation temperature which is also reflected in the microstructure (Figure 2). It has recently been shown [6] that microalloy precipitates in HSLA steels retard the progression of primary Lüders bands, promoting the formation of secondary bands. Accordingly, increasing particle number density and thus precipitation strengthening extends Lüders elongation. The data obtained with the current HSLA steels fully confirm this correlation as is evidenced by Figure 8b and further substantiates the validity of the practiced analysis method.

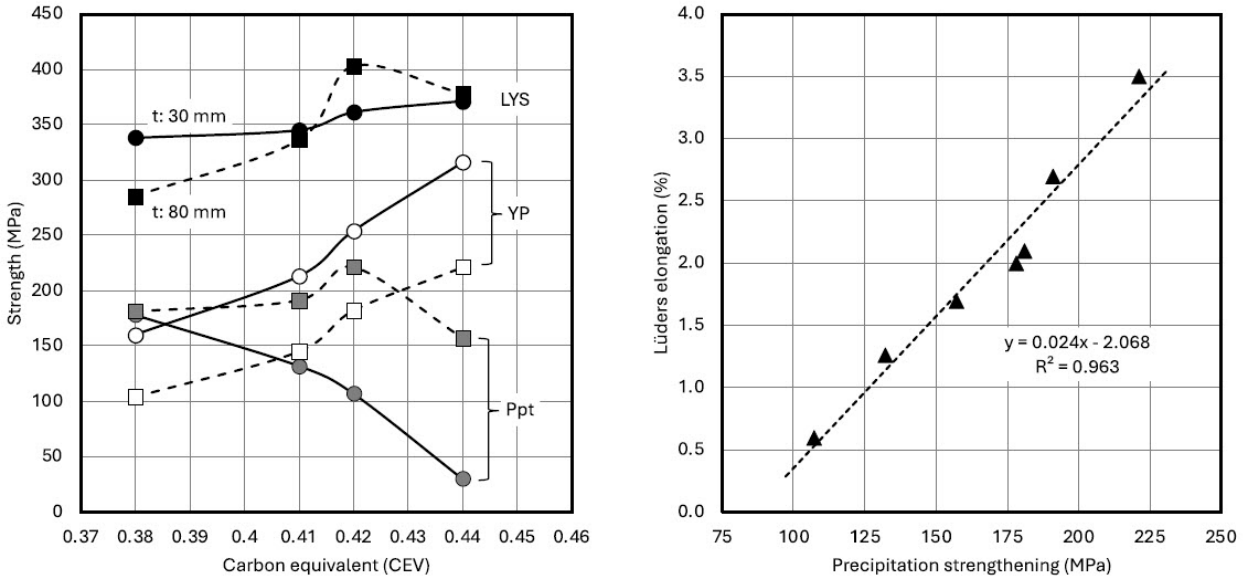

Figure 8: (a) Evaluation of the yielding behavior of the as-rolled steels acc. to [6] identifying the yield point (YP), lower yield strength (LYS) and precipitation (Ppt) strengthening; (b) Correlation between Lüders elongation and precipitation strengthening with linear regression fit.

Lowering the carbon content and increasing the level of the austenite stabilizing elements Ni, Cu, and Mn in alloys 2–4 does not substantially change the volume fraction of proeutectoid ferrite, which is 70–80% in all investigated plates. However, with higher Ni and Cu content, the enriched austenite transforms rather into LTT phases than into pearlite. The LTT phases induce an enhanced dislocation density as noticed in the tensile behavior. Alloy 3 and especially alloy 4 exhibit coarse carbon-rich particles decorating the boundaries of ferrite grains in the 30 mm plates which likely cause the lower toughness performance despite the finer average grain size. The processing of the 80 mm plates involves less austenite deformation and a slower cooling rate after finish rolling, making the transformation more uniform featuring thus suppressing carbon partitioning as a mechanism for the formation of unwanted hard phases. The observed yielding and toughness characteristics support this hypothesis.

Upon full re-austenitizing during a weld cycle, nickel is known to retard the nucleation and growth kinetics of grain boundary ferrite, refine the microstructure, and increase the share of acicular ferrite at the expense of grain boundary ferrite in the CGHAZ, as was reported by Wang et al. [9]. These features can also be recognized in the current steels, for instance when comparing the CGHAZ of alloy 1 (Figure 5b) with that of alloy 4 (Figure 5c). It appears, however, that the benefit of nickel alloying is not so much related to austenite refinement, but rather to an optimization of microstructural features developing within the prior austenite grains upon transformation. With increasing nickel and decreasing carbon content, the microstructure changes from a mix of granular plus upper bainite to pure upper bainite with a reduced fraction of carbon-rich islands (retained austenite and MA). In that sense, a higher nickel content, lowering the transformation temperature, makes the transformation more complete and uniform, thus suppressing carbon partitioning as a mechanism for the formation of unwanted hard phases. Furthermore, a higher nickel content has been reported [10] to change the configuration of the Bain groups in the crystallographic packet within the prior austenite grain while the density of high-angle boundaries remains almost the same. Apparently, these features are not only controlled by the nickel content but also by the welding conditions, i.e., heat input and cooling rate. The thinner gaged plates welded at a lower heat input showed clearly improved HAZ properties already for a lower nickel content of 0.3 percent. The heavier gaged plates obviously require higher nickel addition for achieving significant HAZ property improvement.

The observed positive effect of nickel alloying on the CTOD value in the CGHAZ at -20°C is supported by results from former investigations on the fracture mechanical behavior after welding of steels with similar alloy compositions. The comparison in Figure 9 [11–14] summarizes data reported for the plate thickness range of 25−35 mm confirming that the CTOD-value basically increases with adding nickel up to around 0.3 mass%. Correlation calculations carried out in addition allowed extracting the partial influences of individual parameters from the complex effect on the CTOD value. Accordingly, nickel alloying as well as niobium microalloying clearly showed individual positive effects independent from other influencing parameters. Quantitatively, the positive effect of nickel alloying increases with the plate gage. The CTOD value can be raised by around 0.1 mm in the gage range of 25−35 mm and by around 0.3 mm for gages larger than 70 mm per 0.1 mass% Ni added, respectively.

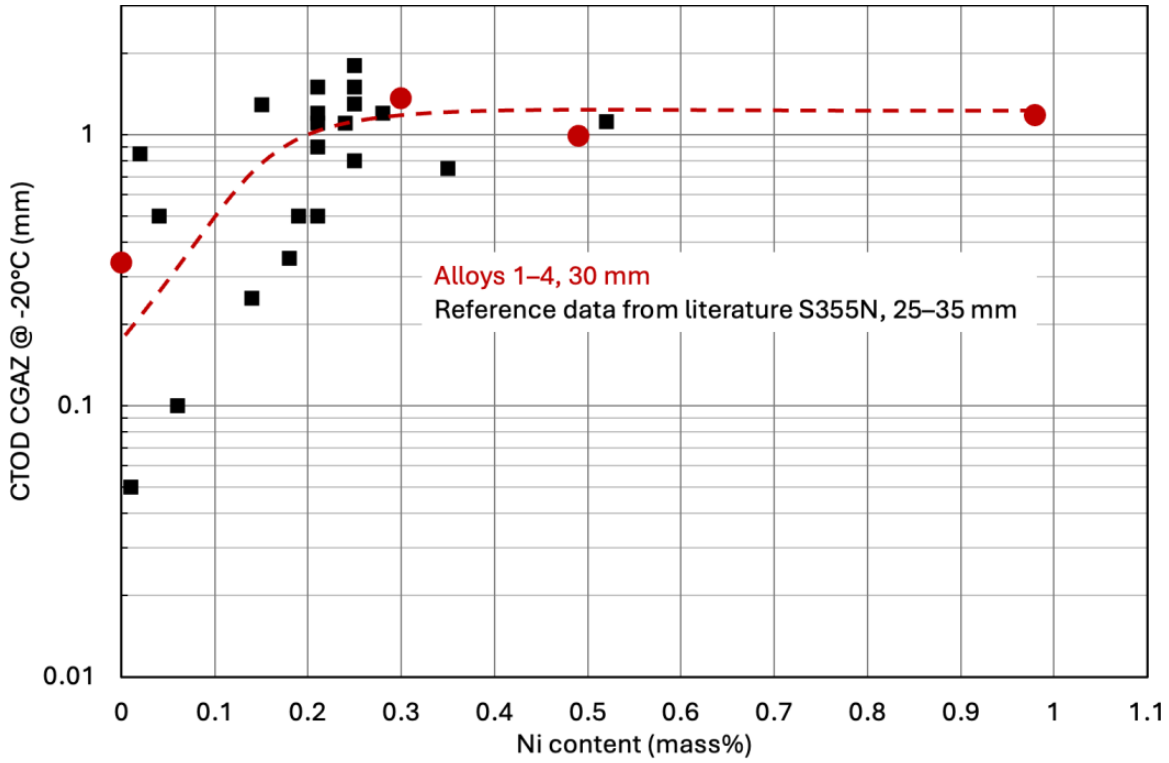

Figure 9: Effect of nickel alloying on CTOD CGHAZ at -20 °C in normalized steel S355 (plate thickness 25–35 mm, black squares [11–14]) in comparison to the current alloys 1–4 for 30 mm plate gage (red circles).

Since in all investigated steels of this study nickel was co-alloyed with copper, the potential effects of the latter must be considered as well. The HAZ data (Figure 7) suggest that the addition of 0.5 mass% Cu might result in a performance loss if the nickel content is too low. Previous CTOD results [1] on similar HSLA plate steels support this concern necessitating a more detailed investigation of the copper-related impact on toughness properties. The same study [1] indicated that the achieved improvement in CTOD can significantly increase the residual fatigue lifetime after appearance of an initial crack. Based on the data shown in Figure 9 the achievable fatigue lifetime extension by nickel alloying should be in the range of 10–15 percent.

CONCLUSIONS

The impact of nickel in association with copper alloying on the properties of microalloyed HSLA plate steel was investigated in this study. The as-rolled steel experiences a strength increase when raising the nickel alloy content, even when significantly lowering the carbon content. Thereby, nickel directly contributes to strength by solid solution and grain refinement. The grain refinement is due to a lower transformation temperature and the resulting increased ferrite nucleation rate. This effect can compensate for lacking austenite conditioning when rolling very heavy plate gages. In this situation, niobium was found to contribute to strength mainly by precipitation. Nickel appeared to have an influence on the magnitude of precipitation strengthening. When combined with a higher cooling rate (thinner plate gage), the delay of austenite transformation can lead to incomplete niobium precipitation causing a reduced strength contribution. At a slower cooling rate (or heavier plate gage), in contrast, a particular nickel content can maximize niobium precipitation strengthening probably by adjusting the transformation temperature to that of the precipitation sweet spot. The present data confirmed a previous finding, suggesting that the magnitude of precipitation strengthening directly correlates with the Lüders elongation. Higher nickel content in association with sufficiently fast cooling rate produces carbon-rich hard phases that can ultimately result in continuous yielding behavior. The presence of such phases deteriorates Charpy toughness. The optimum nickel addition adapted to plate thickness and/or cooling rate provides high toughness at -60 °C even in mid-thickness plate position. Nickel alloying also improves heat affected zone properties. Again, the optimum addition depends on the cooling rate and/or heat input as well as plate thickness. Charpy toughness and CTOD are principally similarly influenced by the nickel content. The results indicate that a higher level of copper alloying can deteriorate these properties if not counteracted by an appropriately high nickel addition.

REFERENCES

1. H. Mohrbacher and A. Kern, On the Effect of Nickel Alloying for Improving the Brittle Fracture Resistance of Structural Plate Steels, AIST transactions. Iron and Steel Technology, to be published April 2025.
2. H. Mohrbacher and A. Kern, Nickel Alloying in Carbon Steel: Fundamentals and Applications, Alloys 2023, 2, pp 1– 28, https://doi.org/10.3390/alloys2010001.
3. I. Kosazu, Overview of Accelerated Cooling of Plate. In Proceedings of the International Conference on Accelerated Cooling of Steel, Southwick, P.D., Ed.; The Metallurgical Society: Pittsburgh, USA, 1986; pp 15–31.
4. B. Graville, A survey review of weld metal hydrogen cracking, Weld World 24(9/10), 1986, pp 190–198.
5. F. B. Pickering, Physical metallurgy and the design of steels, Applied Science Publishers, 1978.
6. H. Mohrbacher, M. Ploberger, G. Ischia, S. Gialanella, T. Hebesberger, Annealing response and yielding behavior of cold rolled advanced HSLA steels, Materials Science and Engineering: A, Volume 903, 2024, 146666. doi.org/10.1016/j.msea.2024.146666
7. H. Mohrbacher, Novel Aspects of Niobium Precipitation in Plate Steels, 3rd Int. Symp. on Recent Developments in Plate Steels Proceedings, AIST, Vail 2024, pp 13–19.
8. M.A. Altuna, A. Iza-Mendia, I. Gutiérrez, Precipitation of Nb in Ferrite After Austenite Conditioning. Part II: Strengthening Contribution in High-Strength Low-Alloy (HSLA) Steels, Metall Mater Trans A 43, 2012, pp4571– 4586. https://doi.org/10.1007/s11661-012-1270-x
9. Z.Q. Wang, X.L. Wang, Y.R. Nan, C.J. Shang, X.M. Wang, K. Liu, B. Chen, Effect of Ni content on the microstructure and mechanical properties of weld metal with both-side submerged arc welding technique, Materials Characterization 138, 2018, pp 67–77. doi.org/10.1016/j.matchar.2018.01.039
10. Y. You, C.J. Shang, S. Subramanian, Effect of Ni Addition on Toughness and Microstructure Evolution in Coarse Grain Heat Affected Zone, Met. Mater. Int., Vol. 20, No. 4, 2014, pp 659–668. https://doi:10.1007/s12540-014- 4011-4
11. P.L. Harrison, P.H.M. Hart, HAZ Toughness of Thick Section Steels, The Welding Institute (TWI) Report No 5543/19/86 and 5543/41/88, 1986 – 1988.
12. T. Haze, Y. Ohio, Y. Kawashima, R. Chijiiwa, S. Aikara, K. Uchino, Y. Tomita, H. Timura, Steel Plates with Superior HAZ Toughness for Offshore Structures, Nippon Steel Technical Report, No. 36, 1988, pp 39–48.
13. D. Uwer, H. Wegmann, J. Adams, Erfahrungen mit dem Verarbeiten eines Offshorestahles, Schweißen und Schneiden, 5/87, 1987, IIW Doc. IX-1455-86, Dezember 1986, pp 1–4.
14. W. Dahl, R. Hubo, B. Müsgen, H.J. Kaiser, G. Sedlacek, J. Bild, Bewertung bruchmechanischer Versagenskonzepte im Hinblick auf eine zuverlässige Vorhersage des Bauteilverhaltens, Studiengesellschaft Stahlanwendung, e.V. , Projekt 137, 1990.

